(2)

Use of Depletion Edge Translation for High-Speed Modulation and Switching of Lightwaves

AFOSR #85-0323 - FINAL REPORT
3/1/88-4/30/89

by
L.A. Coldren: Principal Investigator
T.R. Hausken, R.J. Simes
and R.H. Yan: Students

ECE Technical Report #89-01

DEPARTMENT OF ELECTRICAL AND COMPUTER ENGINEERING
UNIVERSITY OF CALIFORNIA SANTA BARBARA, CALIFORNIA 93106

DD FORM 1473 ATTACHED TO BACK OF THIS SHEET.

(2)

Use of Depletion Edge Translation for High-Speed Modulation and Switching of Lightwaves

AFOSR #85-0323 - FINAL REPORT

3/1/88-4/30/89

by

L.A. Coldren: Principal Investigator
T.R. Hausken, R.J. Simes
and R.H. Yan: Students

ECE Technical Report #89-01

Department of Electrical & Computer Engineering

University of California at Santa Barbara

May 1989

SECURITY CLASSIFICATION OF THIS PAGE

REPORT DOCUMENTATION PAGE

1a. REPORT SECURITY CLASSIFICATION: UNCLASSIFIED	1b. RESTRICTIVE MARKINGS
2a. SECURITY CLASSIFICATION AUTHORITY	3. DISTRIBUTION / AVAILABILITY OF REPORT: Approved for public release; distribution unlimited.
2b. DECLASSIFICATION / DOWNGRADING SCHEDULE	
4. PERFORMING ORGANIZATION REPORT NUMBER(S)	5. MONITORING ORGANIZATION REPORT NUMBER(S): AFOSR-TR- 89-1054
6a. NAME OF PERFORMING ORGANIZATION: UNIVERSITY OF CALIFORNIA; 6b. OFFICE SYMBOL (If applicable)	7a. NAME OF MONITORING ORGANIZATION: AFOSR
6c. ADDRESS (City, State, and ZIP Code): DEPT. OF LECTRICAL & COMPUTER ENGINEERING, UNIVERSITY OF CALIFORNIA, SANTA BARBARA, CA 93106	7b. ADDRESS (City, State, and ZIP Code): BOLLING AFB, DC 20332-6448
8a. NAME OF FUNDING / SPONSORING ORGANIZATION: AFOSR; 8b. OFFICE SYMBOL (If applicable): NE	9. PROCUREMENT INSTRUMENT IDENTIFICATION NUMBER: AFOSR-85-0323
8c. ADDRESS (City, State, and ZIP Code): BUILDING 410, BOLLING AFB, DC 20332-6448	10. SOURCE OF FUNDING NUMBERS: PROGRAM ELEMENT NO. 61102F; PROJECT NO. 2305; TASK NO. B4; WORK UNIT ACCESSION NO.

11. TITLE (Include Security Classification)
USE OF DEPLETION EDGE TRANSLATION FOR HIGH SPEED MODULATION AND SWITCHING OF LIGHTWAVES (UNCLASSIFIED)

12. PERSONAL AUTHOR(S)
LARRY A. COLDREN

13a. TYPE OF REPORT	13b. TIME COVERED	14. DATE OF REPORT (Year, Month, Day)	15. PAGE COUNT
FINAL	FROM 3/1/88 TO 4/30/89	890531	32

16. SUPPLEMENTARY NOTATION

17. COSATI CODES			18. SUBJECT TERMS (Continue on reverse if necessary and identify by block number)
FIELD	GROUP	SUB-GROUP	OPTICAL MODULATORS & COMPUTING, MULTI QUANTUM-WELL MODULATORS, SURFACE EMITTING LASERS & MODULATORS, SPATIAL LIGHT MODULATORS

19. ABSTRACT (Continue on reverse if necessary and identify by block number)

We report on our work for the period 1 March 1988 to 28 February 1989. The primary emphasis has been the Fabry-Perot modulator which we introduced in last year's interim report. Over the past year, we have completed the design, optimization and sensitivity analysis for the modulator. Experimentally, we have made good progress in improving the device performance going from a 2:1 on:off ratio for a 25 V drive to a 10:1 on:off ratio for a 7 V drive. In section V.3 of the present report, we present a brief comparison of our modulator results with those of other groups.

With supplemental support from other contracts, we have also made significant advances in fundamental areas which should open new avenues for continued improvement of existing devices and lead to new device structures. We have observed a new effect in superlattices—Field-Induced Stark Localization—which leads to a blue-shift in absorption edge rather than a conventional red shift. We have also observed optical properties ascribable only to quantum wire effects in quantum wire structures grown directly by molecular beam epitaxy using a process pioneered at UCSB. Both of these new structures should prove to be promising active regions for the Fabry-Perot device. Additionally, the Fabry-Perot will serve as an excellent vehicle with which to fully characterize the electro-optic properties of these new structures.

20. DISTRIBUTION / AVAILABILITY OF ABSTRACT: ☒ UNCLASSIFIED/UNLIMITED ☐ SAME AS RPT. ☐ DTIC USERS	21. ABSTRACT SECURITY CLASSIFICATION: UNCLASSIFIED
22a. NAME OF RESPONSIBLE INDIVIDUAL: DR. LEE GILES	22b. TELEPHONE (Include Area Code): (202) 767-4931; 22c. OFFICE SYMBOL: NE

DD FORM 1473, 84 MAR — 83 APR edition may be used until exhausted. All other editions are obsolete.

SECURITY CLASSIFICATION OF THIS PAGE

II. Summary

We report on our work for the period 1 March 1988 to 28 February 1989. The primary emphasis has been the Fabry-Perot modulator which we introduced in last year's interim report. Over the past year, we have completed the design, optimization and sensitivity analysis for the modulator. Experimentally, we have made good progress in improving the device performance going from a 2:1 on:off ratio for a 25 V drive to a 10:1 on:off ratio for a 7 V drive. In section V.3 of the present report, we present a brief comparison of our modulator results with those of other groups.

With supplemental support from other contracts, we have also made significant advances in fundamental areas which should open new avenues for continued improvement of existing devices and lead to new device structures. We have observed a new effect in superlattices—Field-Induced Stark Localization—which leads to a blue-shift in absorption edge rather than a conventional red shift. We have also observed optical properties ascribable only to quantum wire effects in quantum wire structures grown directly by molecular beam epitaxy using a process pioneered at UCSB. Both of these new structures should prove to be promising active regions for the Fabry-Perot device. Additionally, the Fabry-Perot will serve as an excellent vehicle with which to fully characterize the electro-optic properties of these new structures.

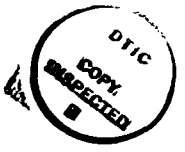

III. Introduction

III.1. Overview

Surface-normal light modulators have drawn considerable interest because of their potential applications in optical processing and interconnection. The modulation mechanisms can be divided into two categories: optical and electronic. The optical-optical type of operation can be used for modulators as well as logic gates, initial studies have been aimed at [1-3]. On the other hand, light modulation can also be achieved by electronic means [4-8]. Although the whole structure can be made in a single epitaxial growth, the total length is usually only a few μm's, so methods of making the interaction length longer are adapted. Fig. 1(a) is an example for the absorption modulators [5]. A grating mirror is placed under the active region so that the light can be reflected and the interaction length is doubled, compared with the case without the grating. Fig. 1(b) is a Fabry-Perot modulator [7-11] which is the building block of the present research work. Two grating mirrors are used to provide multiple reflections and therefore to

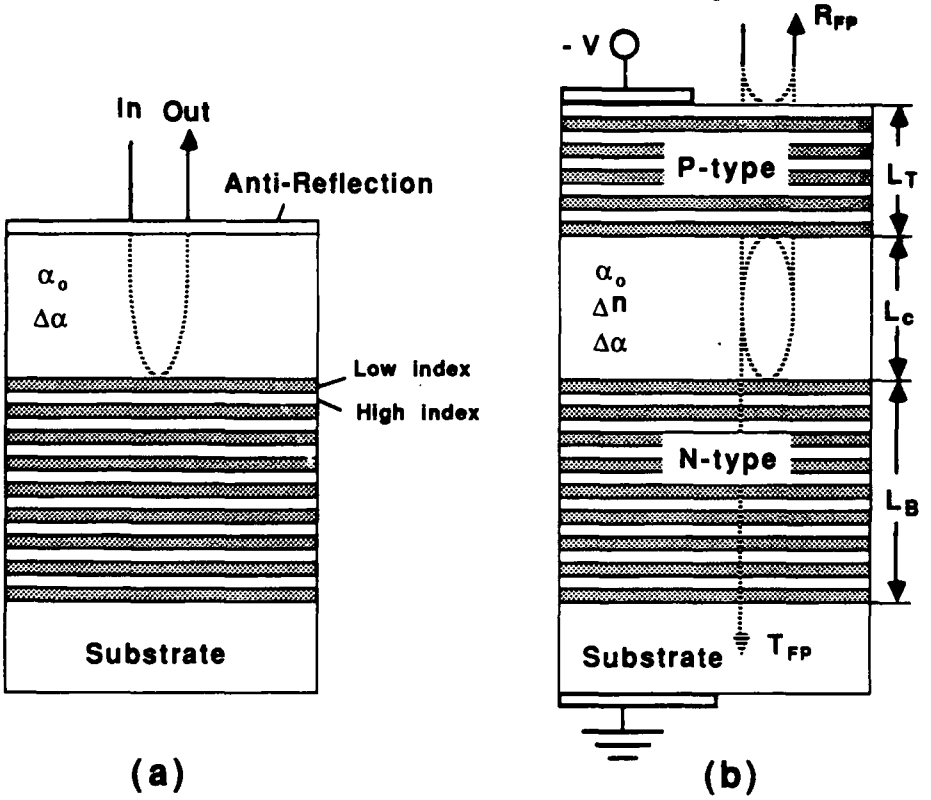

Figure 1 Schematic drawing of surface normal modulators (a) absorption modulator, and (b) Fabry-Perot modulator. Grating mirrors are adapted to enhance the interaction length. The absorption modulator can be implemented as a reflection or transmission modulator with or without the grating, respectively. The Fabry-Perot modulator can be used as both types of modulators as long as the transmitted signal can be collected.

increase the interaction length by many times the active region length so the modulation efficiency is greatly enhanced. Both absorption and index modulation can be used for intensity modulation in these structures [12]. Our initial work has been focusing on the index-tuning dominant operation. Modulation efficiency up to $\Delta R/V=10\%$ per volt is achieved. Although the bandwidth is somewhat limited due to high-Q cavities adapted in these devices, asymmetric Fabry-Perot (ASFP) modulators with comparable efficiency but wider bandwidth are currently under investigation. These ASFP modulators use absorption to balance the resonator for high contrast; and as a result, the Q is lowered and the bandwidth is increased[13].

III.2. Fabry-Perot Resonator/Modulator Operating Principles

A Fabry-Perot cavity is formed by inserting a spacer layer between two Bragg reflectors. The thickness and refractive index of the cavity, together with the phase of Bragg reflectors determine the positions of the resonant wavelength. The entire structure of the Fabry-Perot resonator can be grown monolithically, e.g. by molecular beam epitaxy (MBE); the Bragg reflector is basically a quarter wavelength stack of alternating layers with different refractive indices, e.g., AlAs and AlGaAs [14,15].

The reflectivity of the Bragg reflector is a function of the index difference as well as the total number of layers in the dielectric stack. Fig. 2a shows the reflection spectrum of two different AlAs/$Al_{0.2}Ga_{0.8}As$ gratings. The air interface has a large refractive index discontinuity and can help the reflection by appropriate design of the layer structures, i.e., the interface is formed with the higher index layer. The 5-period grating with the air interface has the same reflectivity as the $8^1/_2$-period grating. As the number of periods increases, the reflectivity at the Bragg wavelength increases. Fig. 2b is the calculated reflectivity as a function of the grating length at a Bragg wavelength of 0.87 μm [16]. The mirrors are all assumed to be made of alternating quarter wavelength layers of AlAs and $Al_{0.2}Ga_{0.8}$ As. The top curve with open circles is the case of the top grating of the Fabry-Perot resonator with an air interface on the top and the multiple quantum well (MQW) region on the bottom. The bottom curve with open triangles is the case of the bottom grating with the MQW region on the top and the GaAs substrate on the bottom. The calculation is done by using the Transmission Matrix Method [17], and the material parameters used in the calculation are listed in Table I.

The reflection spectrum for a Fabry-Perot structure with gratings of Fig. 2a and an active

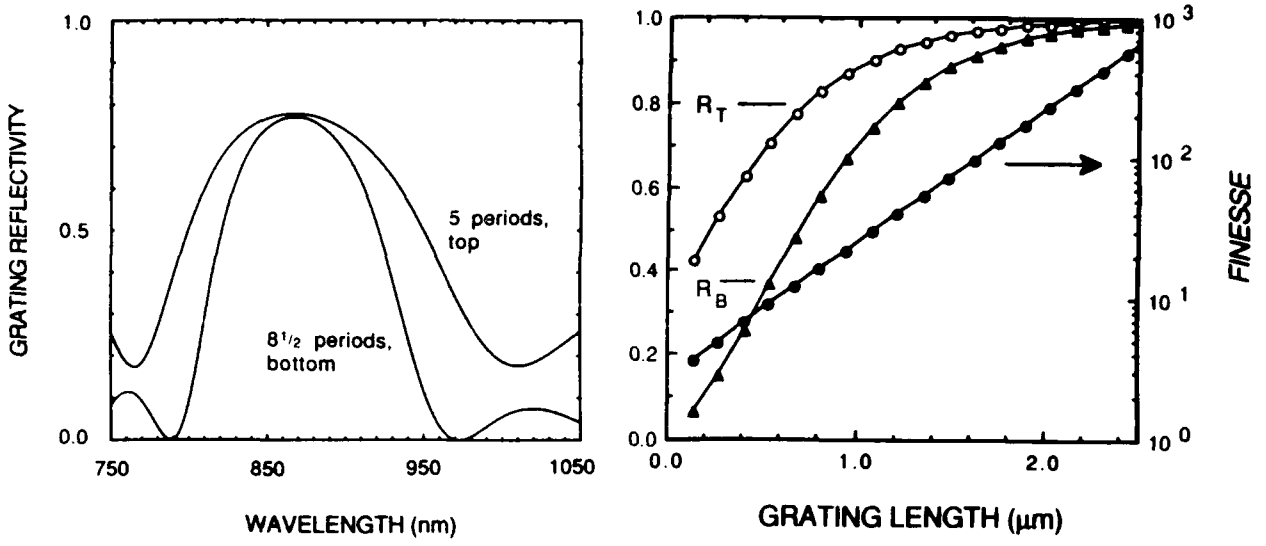

Figure 2 (a) Reflectivity spectrum of two different gratings. The top curve shows a 5 periods grating with an air interface on top, and multiple quantum well material on the bottom. The grating is made of alternating quarter wavelength $Al_{0.2}Ga_{0.8}As$ and AlAs layers, starting with AlAs near the substrate. The bottom curve is a $8^1/_2$ periods grating (the extra half period is a quarter wavelength AlAs layer). The grating is buried between the GaAs substrate and multiple quantum well material. (b) Reflectivity as a function of the grating length. The relevant values are listed in Table I. The top curve with open circles is for the top grating; the bottom curve with open triangles is for the bottom grating. The line with solid circles is the *finesse*, F defined as $\pi\sqrt{R_T}/(1-R_T)$, as Eq.(4').

region of ~2.0 μm of 100Å GaAs quantum wells with 100Å $Al_{0.2}Ga_{0.8}As$ barriers is shown in Fig. 3a. The calculated spectrum is shown in Fig. 3b. The refractive indices were taken from

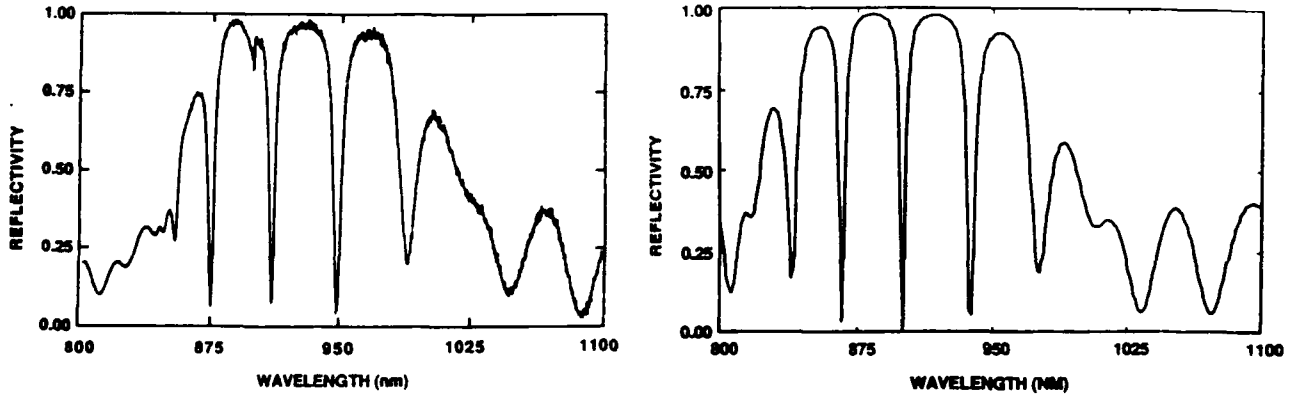

Figure 3 (a) Wide band spectra of Device #1. The layer structure is described in Section V.1. (b) The calculated spectrum using the Transmission Matrix Method.

Table I Material parameters in the gratings.

PARAMETER	SYMBOL	VALUE
Wavelength	λ	0.87μm
High index in the grating	n_H	3.458
Low index in the grating	n_L	2.983
Index of the substrate	n_S	3.534

Ref.[18]. The grown sample has the expected behavior by comparing the two figures. As can be seen, there are several Fabry-Perot resonant modes within the stop band of the grating mirrors. Ideally, the minima should go to zero if the cavity is balanced; we have measured minima as low as 3.2%. One method of modulation is to change (increase) the loss in the cavity. The absorption would reduce the finesse of the resonator to move the mode peak up and down. Another method is to change the refractive index in the Fabry-Perot cavity. When the index of the cavity is changed, the interference spectrum, and thus the reflectivity at a particular wavelength, changes. Fig. 4 illustrates the tuning behavior. As the voltage is applied across the spacer layer (the top grating is doped p-type and the bottom grating is doped n-type.), the index is increased and the spectrum shifts to the longer wavelength side. The higher the grating reflectivity is, the sharper the resonant modes is (or the higher the finesse is)

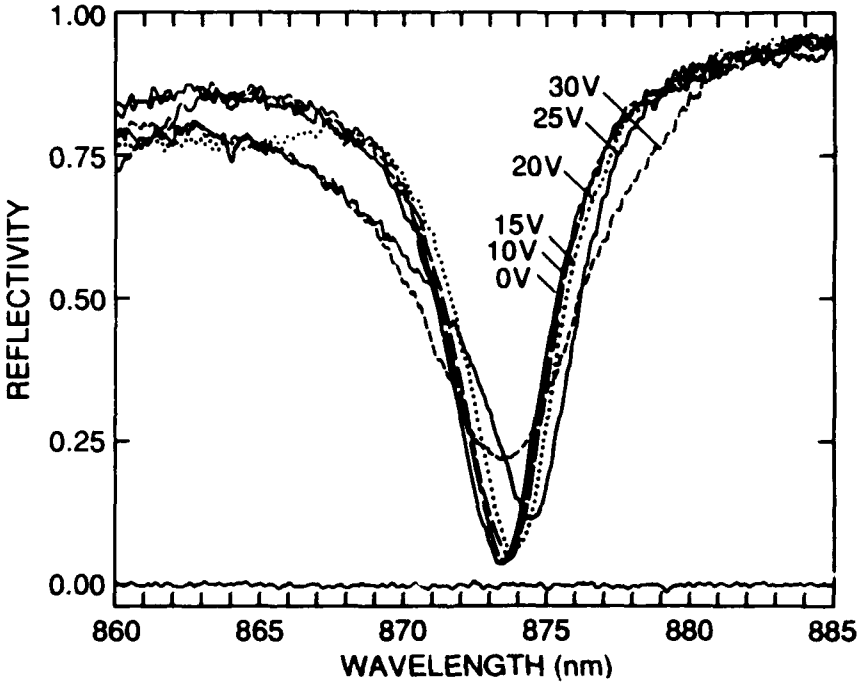

Figure 4 Narrow band spectra of Device #1 under different bias voltages. The shift of the resonant mode is used to estimate the index shift; the reflectivity at the resonant mode under electric fields is used to estimate the associated absorption change. An 8:1 on/off ratio is observed near 873 nm.

and . ·refore, the more reflectivity modulation can be achieved for a given index shift. An on/·.f ratio of 8:1 (a modulation depth close to 90%) is observed in Fig. 4 for 25 V at 873 nm.

To date, only reflection modulators have been reported with monolithically grown Fabry-Perot structures, because the material systems used are GaAs/AlGaAs with opaque GaAs substrates [7,8]. The mirror design is asymmetrical. By removing the substrate and using a pair of symmetric mirrors, one could construct a Fabry-Perot modulator, as both a reflection and transmission modulator. On the other hand, with a transparent substrate, e.g. InP and the related quartenary compounds or GaAs with InGaAs/GaAs strained quantum wells as the active media, an asymmetric mirror pair can be used to construct both reflection and transmission modulators without removing the substrate [9]. These could be especially interesting since the two outputs are complementary to each other; the device could be used as a true optical switch.

IV. Theory

IV.1. Design of Surface-Normal Fabry-Perot Electro-Optic Modulator

The optimization of the reflectivity modulation, and the sensitivity of the performance on the operating conditions are discussed in this section through the use of a set of design equations which, with experimental justifications, relate the refractive index shift, absorption change, cavity length and grating properties of Fabry-Perot modulators with GaAs/AlGaAs multiple quantum well active regions. In the high Q cavities, the modulation is found to be mainly determined by the index shift, and less sensitive to the accompanying absorption change for a chirp greater than one; while the modulation can also be obtained via absorption modulation when the chirp is small. However, the residual loss in the cavity should be kept lower than 500 cm^{-1} in order for the reflectivity modulation to be at least 50%. With a *finesse* of 40, the optimized cavity is found to be approximately three times the optical wavelength with an operating voltage of 7-10 volts for the multiple quantum well material to achieve a 50% reflectivity modulation. In the following, we are going to use a simple scattering matrix method to analytically study the electro-optic modulation properties of the Fabry-Perot structure. As indicated in Fig. 1(b), the design parameters of Fabry-Perot modulators consist of the grating mirror length L_T; L_B, the cavity length L_c and the applied voltage V. The tuning of the reflection R_{FP} and the transmission T_{FP} is affected by the electro-optical properties of the active region as well as the Fabry-Perot structure itself.

By using the scattering matrices of both the top and bottom grating as shown schematically in Fig. 5, we could express the effective reflection (transmission), R_{FP} (T_{FP}) of the Fabry-

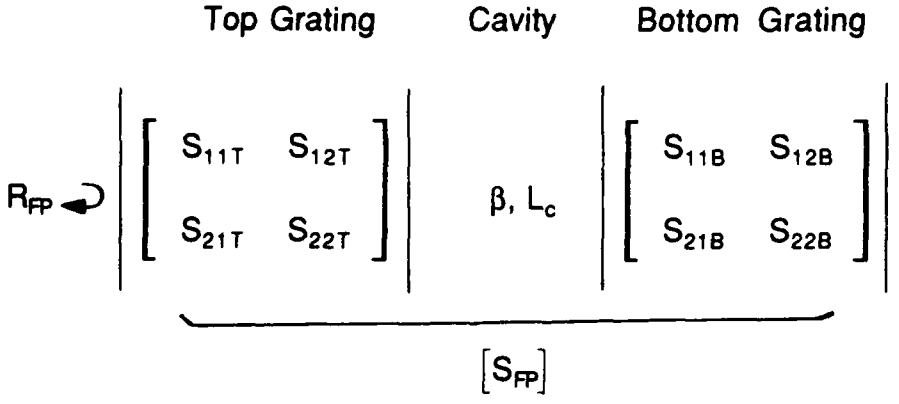

Figure 5 Illustration of the scattering matrices in deriving design equations.

Perot, at least at the Bragg wavelength of the gratings, by the following well-known expressions,

$$R_{FP} = |S_{11FP}|^2 = \left| \frac{S_{11T} - S_{11B} e^{j\theta} (S_{11T} S_{22T} - S_{21T} S_{12T})}{1 - S_{22T} S_{11B} e^{j\theta}} \right|^2, \quad (1a)$$

and

$$T_{FP} = |S_{12FP}|^2 = \left| \frac{S_{12T} S_{12B} e^{j\theta/2}}{1 - S_{22T} S_{11B} e^{j\theta}} \right|^2, \quad (1b)$$

where we have used the notations in [19]. Subscripts T, B and FP stand for top, bottom and Fabry-Perot. The phase θ is the propagation constant β (may be a complex value) times the round-trip cavity length, $2L_c$. The idea of the modulation is to change the phase θ by

$$\Delta\theta = \Delta\theta_r + j\Delta\theta_i, \quad (2)$$

where $\Delta\theta_r = 4\pi\Delta n L_c/\lambda$ and $\Delta\theta_i = \Delta\alpha \cdot L_c$ in which Δn and $\Delta\alpha$ are the index and absorption shift of the cavity, respectively. λ is the free space wavelength. It should be noted that if Eqs.(1) and (2) are used at the Bragg wavelength, the Transmission Matrix Method gives the same result. For the resonator to operate in the reflection mode, a low reflection resonance is desired to provide a low enough off level, and this can be achieved by requiring the numerator of Eq.(1a) to be zero:

$$S_{11T} - S_{11B} e^{j\theta} (S_{11T} S_{22T} - S_{21T} S_{12T}) = 0 \quad (3)$$

Since the substrate has a very different refractive index from that of the air, either a pair of identical mirrors can be used with the substrate removed, or different periods of grating mirrors should be used to provide the same reflectivities without removing the substrate. The general idea is to use extra periods in the bottom grating to balance the contribution from the air interface. Fig. 2a provides such an example.

The gratings are made of materials with absorption edges far away from the operating photon energy, so the absorption is presumably negligible. This leads to the condition of $|S_{11T}S_{22T} - S_{12T}S_{21T}|=1$. Therefore, Eq.(3) can be rewritten as

$$R_T = \exp(-2\alpha_o L_c)\, R_B, \qquad (4)$$

where the cavity has a residual loss, α_o and we have used R to replace $|S_{11}|^2$. Under the assumption of negligible grating loss, Eq.(4) also maximizes the transmission in Eq.(1b) for any given R_B and α_o. Therefore, Eq.(4) can be viewed as a *Cavity Design Equation* for both reflection and transmission modulators.

The *finesse*, F, defined as the ratio of free space mode spacing to the FWHM of the mode by assuming a uniform refractive index, is useful for the discussion of the modulation. Using Eqs.(1) and under the condition of Eq.(4), we have

$$F = \frac{\pi\sqrt{R_T}}{1 - R_T}, \qquad (4')$$

$$= \frac{\pi\sqrt{R_B}}{e^{\alpha_o L_c} - R_B e^{-\alpha_o L_c}}.$$

The first line has the same form as the conventional expression for the *finesse* [19]. The measured *finesse* of the epitaxial Fabry-Perot would be different from F when the material dispersion ($dn/d\lambda$) is not uniform. Fig. 2b also plots F as a function of the top grating length.

The Fabry-Perot modulator is designed to have zero reflection (and thus maximum transmission) at the Bragg condition before any index shift is applied. From Eqs.(1), for an index shift of Δn and absorption change of $\Delta\alpha$, the reflection and transmission are

$$R_{FP} \approx \frac{1 + \frac{4}{\alpha_c^2}}{1 + \left(\frac{\pi}{\Delta\Theta} + \frac{4}{\alpha_c}\right)^2}, \qquad (5)$$

and

$$T_{FP} \approx \frac{\left(\frac{\pi}{\Delta\Theta}\right)^2 \exp(-\alpha_o L_c)}{1 + \left(\frac{\pi}{\Delta\Theta} + \frac{1}{\alpha_c}\right)^2}, \qquad (6)$$

respectively. In the above derivation, we have used a chirp parameter $\alpha_c = 4\pi\Delta n/(\lambda\Delta\alpha)$ to relate the index and absorption change, and both Δn and $\Delta\alpha$ are assumed to be small. $\Delta\Theta = \Delta\theta_r \cdot F$ is the effective phase shift which indicates the enhancement of $\Delta\theta_r$ through the

finesse F of the cavity. When $\Delta\Theta=\pi$, Δn corresponds to the amount of index shift required to shift the mode by half of the FWHM of the resonance. Ideally, i.e., $\alpha_c \rightarrow \infty$, such a shift would lead to a 50% reflection change, and the sum of R_{FP} and T_{FP} equals unity for zero cavity loss. Eqs.(5) and (6) are the *Modulation Design Equations*, which give the modulation as functions of the cavity parameters, L_c and F, as well as the active medium properties, Δn and α_c. Although the modulation depends on R_T, we have used $R_T \approx 1$ which leads to the final approximation. In general, it is desired to tune R_{FP} (T_{FP}) to be as high (low) as possible.

We have plotted Eq.(5) and (6) as dashed and dotted curves in Fig.6. The horizontal axis

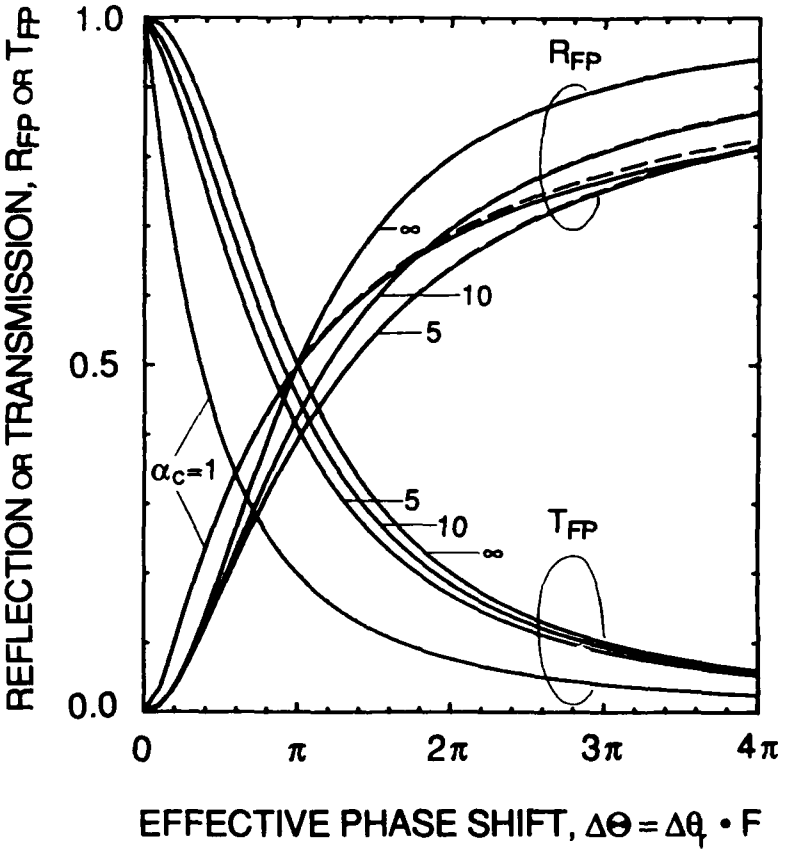

Figure 6 Reflection and transmission modulation versus $\Delta\Theta=4L_C\Delta nF/\lambda$ with different chirp parameters. The dotted lines are for the transmission from Eq.(6), while the dashed lines are for the reflection from Eq.(5). The solid lines are calculations using the exact expressions of Eqs.(1). We have ignored the residual loss in the cavity, so the actual transmission would be lowered by a factor of $\exp(-\alpha_o L_c)$ The approximation of Eq.(1b) by Eq.(6) is very good. Eg.(5) is also a good approximation of Eq.(1a), although the deviation is noticeable for $\alpha_c=1$ when the modulation is large. In the vicinity of $\pi \leq \Delta\Theta \leq 2\pi$, R_{FP} is not sensitive to the chirp. The modulation of T_{FP} is efficient when α_c is close to 1.

is in terms of $\Delta\Theta$. The plot is made with different α_c's. The solid lines are for Eqs.(1a) and (1b) where we assume R_T=0.9. Since the solid and the corresponding dashed and dotted lines in Fig. 6 are almost indistinguishable, we could conclude that Eq.(5) and (6) are good approximations of Eqs.(1a) and (1b), respectively, and the agreement gets even better as R_T approaches one.

It can be noted that when $\alpha_c \approx 1$, R_{FP} and T_{FP} are modulated very effectively for small phase shifts, due to the added absorption. But in the vicinity of $\pi \leq \Delta\Theta \leq 2\pi$, and under the condition of $\alpha_C > 1$, R_{FP} and T_{FP} are almost independent of α_c and are mainly determined by Δn. That is, the reflectivity modulation is quite independent of the simultaneous absorption modulation in high-Q cavities. Therefore, as mentioned earlier, we are concentrating on the index modulation. However, the actual modulation would deviate slightly from the ideal case of pure index modulation. Since R_{FP} and T_{FP} are almost complementary to each other, the optimization of one would lead to the optimization of the other, although the detailed behaviors are somewhat different (although complementary). In reflection modulation, good on/off ratio should be easy to achieve by balancing the mirrors, using Eq.(4); while the insertion loss may be high due to the requirement of large index shift. On the other hand, for transmission modulation, low insertion loss is easily obtained by balancing the mirrors, again using Eq.(4); while a good on/off ratio (modulation depth) requires large index shifts. Since reflection modulators have available experimental data , we are going to concentrate on the discussion of Eq. (5). From the slope of R_{FP} vs. $\Delta\Theta$ in Fig. 6, one tends to conclude that $\pi \leq \Delta\Theta \leq 2\pi$ may be the most efficient region to operate the modulators. We give experimental verifications of Eq. (5) in the following.

IV.2. Design Optimization

Design Equation (5) relates the reflection modulation to the index shift, chirp, cavity length, cavity loss, and mirror reflectivity. Depending upon the imposed constraints, the design equation can be utilized to optimize the device performance. We consider first the cavity itself, and then the optimization with a given bias voltage. Although we are going to concentrate on the design of reflection modulators with MQW active regions, the design equations (4) - (6) are applicable in general.

The Maximum Allowable Cavity Loss

The maximum achievable index shift of MQW is limited as shown by the experiments in the previous sub-section, so we are going to assume a fixed Δn at first. In the case of no residual cavity loss and a fixed chirp parameter, the modulation is determined by the effective phase shift $\Delta\Theta$ which is therefore the quantity to be optimized. In the case of a cavity with some residual loss, α_o, we could use Eq.(4) to express $\Delta\Theta$ as

$$\Delta\Theta = \frac{4\pi\Delta n}{\lambda} L_c \frac{\pi\sqrt{R_B}}{e^{\alpha_o L_c} - R_B e^{-\alpha_o L_c}},$$

$$\approx \frac{4\pi\Delta n}{\lambda} L_c \frac{\pi\sqrt{R_B}}{(1-R_B) + (1+R_B)\alpha_o L_c}. \qquad (7)$$

When $\alpha_o L_c$ becomes much greater than $(1-R_B)/(1+R_B)$, $\Delta\Theta$ approaches a constant value $\Delta\Theta_o$ which is given by,

$$\Delta\Theta_o = \frac{4\pi\Delta n}{\lambda} \frac{\pi\sqrt{R_B}}{(1+R_B)\alpha_0}. \qquad (8)$$

From Fig.6, we know that $\Delta\Theta_o$ should be greater than π to have an efficient modulation. Therefore, α_o should be kept below $500cm^{-1}$ if $\Delta n/n=0.2\%$ and $\lambda=0.87$ μm are assumed. To reach $\Delta\Theta_o$, L_c should be much greater than $(1-R_B)/\alpha_o(1+R_B)$. For a low residual active medium with a modest finesse, it requires a very large L_c to reach $\Delta\Theta_o$ (which would be quite large), and we can therefore ignore the residual loss effect.

Maximizing Modulation per unit Drive Voltage

The next case to consider is to maximize the reflectivity modulation for a given operating voltage, V. The index modulation of a MQW can be well-described by a quadratic electro-optic effect with a limitation on the maximum applicable field,

$$\Delta n = b\left(\frac{V}{L_c}\right)^2, \qquad (9)$$

where $b=Sn^3/2$ with S as the quadratic electro-optic coefficient, and

$$V/L_c \leq E_{max}. \qquad (10)$$

Eq. (10) defines the constraint for the modulators. As shown in Fig. 7, the region to the left of the dashed line indicates the violation of Eq. (10). By Eq.(9), $\Delta\Theta$ can be re-expressed as

$$\Delta\Theta = \frac{4\pi b V^2 F}{\lambda \quad L_c}. \qquad (11)$$

The family curves for various $\Delta\Theta$'s in Fig. 7 show that a small L_c is desired to minimize the required voltage for a given $\Delta\Theta$. However, the maximum applicable field acts as a lower bound of the cavity length, $L_{c,min}=V/E_{max}$. In Fig. 7, we include two different *finesse*, F=40

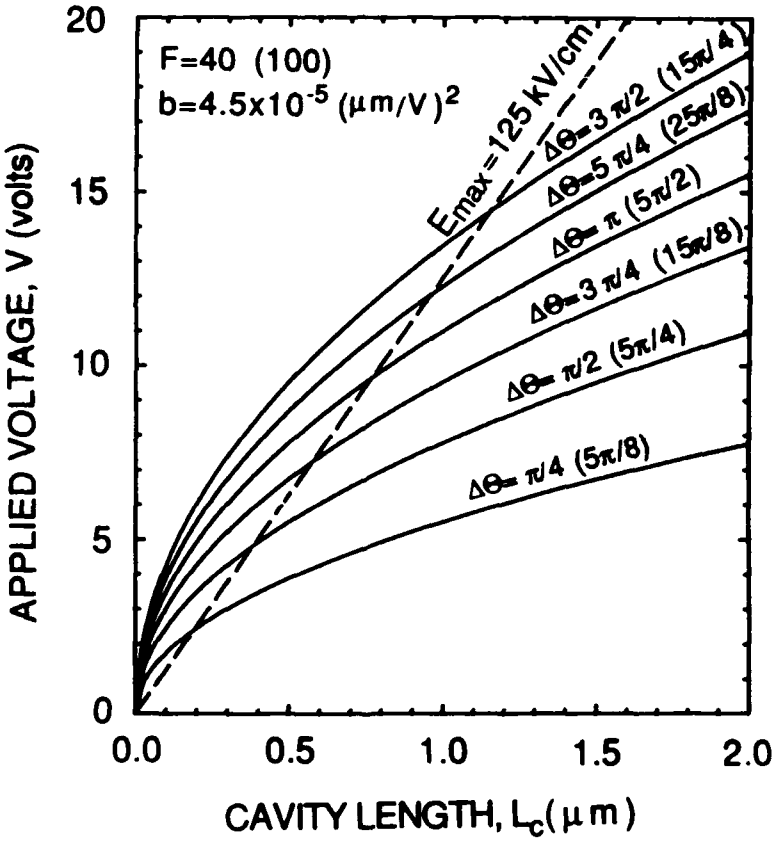

Figure 7 A modulator design map for multiple quantum well active region with quadratic electro-optic effects. The dashed line defines the boundary for maximum applicable fields. The region to the left of the boundary line can not be used due to a negative index shift would actually appear, accompanied by large absorption changes. The solid family curves are constant modulation contours. The numbers of $\Delta\Theta$ listed (in parenthesis) are for a finesse of 40 (100). The simultaneous absorption change is ignored in the calculation because the chirping effect is not important when $\pi \leq \Delta\Theta \leq 2\pi$.

and 100. $b=4.5\times10^{-5}(\mu m/V)^2$ is used for the MQW discussed in the previous section. The intersection of constant $\Delta\Theta$ curves and $E_{max}=V/L_c$ (125kV/cm in this case) represents the required voltage, and the corresponding (minimum) cavity length to achieve such a reflection. For example, L_c of Device #1 is 2.1μm, so a 25 V voltage satisfies the equality of Eq.(10), and gives a $\Delta\Theta$ of 0.7π. In general, the maximum achievable $\Delta\Theta$ as a function of the applied voltage is

$$\Delta\Theta = \frac{4\pi b E_{max}}{\lambda} F V \quad . \tag{12}$$

From Fig. 7, F=40 gives V=10 volts and L_c=0.62 μm for $\Delta\Theta=\pi$; while F=100 gives V=4 volts and L_c=0.35 μm. This latter set of parameters provide a reasonable design for the modulators for both the efficiency and the consideration of sensitivity as discussed below.

IV.3. Sensitivity Analysis

After the discussion in the previous sub-section, one tends to like to use a high finesse Fabry-Perot resonator for the modulation. But the sensitivity to various manufacturing errors and system tolerance also increases as the finesse increases. Actually, the sensitivity goes up quadratically with the finesse, so the knowledge of the refractive index and absorption coefficient, as well as the controllability of the material thickness becomes critical.

First of all, let's look at the effect of a high *finesse* on the desired zero reflectivity before the index shift is applied As mentioned earlier, we must use extra layers, usually around 8~10 in the bottom mirror to balance the strong reflectivity from the air interface. Since the amplitude reflection is given by $(n_H-n_L)/(n_H+n_L)\approx0.074$, a one percent index uncertainty would lead to one percent error in the amplitude reflection coefficient. Therefore, the error in the amplitude reflection coefficient, δr would be approximately, 5×10^{-3} where δr can be view as $r_1=\delta r+\exp(-\alpha_o L_c)r_2$. Furthermore, if there is an uncertainty of $\delta\alpha_o L_c$ in $\alpha_o L_c$, δR, the error of the "zero" reflectivity or the "residual" reflectivity would be, using Eq.(1),

$$\sqrt{\delta R_{FP}} \approx \frac{F}{\pi}\left(\delta r + \delta\alpha_o L\right) , \tag{13}$$

where we have assumed $\sqrt{R_T}\approx1$. For F=10, the above mentioned δr would cause a "residual" reflectivity of less than 0.1%. However, an F of 100 would lead to a 3% residual reflectivity. If we consider the uncertainty of the residual loss, the residual reflectivity would be even

higher. Assuming the uncertainties of δr and $\delta\alpha_o L_c$ add up to 1%, then for δR_{FP} to be less than 5% which would lead to a 10 dB on/off ratio for R_{FP}=50%, F should be no larger than 100. From such minimum reflectivity analysis and Fig. 7, we may conclude that a *finesse* $\leq$100 is suitable for efficient modulation while not so sensitive to the design variations.

Another more strict requirement is the layer growth control and the uniformity. The resonant modes are given by requiring θ in Eq.(1) equal to $2m\pi$ where m is an integer, i.e. $4\pi nL_c/\lambda=2m\pi$. An error in nL_c, δnL_c would lead to an error in the mode position by, $\delta\lambda/\lambda=\delta nL_c/nL_c$. Effectively, δnL_c introduces a "residual" reflectivity caused by the misalignment of the mode if a fixed measured λ is assumed. The residual reflectivity is given by inserting $\Delta\Theta'=4\pi\delta nL_cF/\lambda$ as it were "$\Delta\Theta$" into Eq.(5). From Fig. 6, $\Delta\Theta'$ should be kept below 0.3π to kept δR_{FP} below 5%. If the error is due to the misalignment of the lasing wavelength, $\delta\lambda$, the *finesse* $F=\Delta\Theta'\lambda/(4\pi nL_c\delta\lambda/\lambda)$ is required to be no greater than $200\lambda/nL_c$ if $\delta\lambda\approx$3Å (corresponding to an uncertainty of 0.5 meV in photon energy). Furthermore, if $L_c=\lambda$, F should be smaller than 100. On the other hand, if the error is due to a growth error, then for F=100, the controllability of δnL_c should be within $10^{-3}\lambda$. This latter analysis indicates that although with a finesse of 100, the optimized cavity is found to be approximately one and a half times the optical wavelength with an operating voltage less than 5 volts for quantum well material, the layer thickness control and uniformity are very critical and putting strict requirements on the material growth. By using a wider bandwidth design such as the ASFP proposed in Section III.1, the sensitivity constraints can be largely released, while maintaining comparable efficiency.

V. Experimental Results

V.1. Experimental Justification of Design Equations

Device #1 [7] is composed of 5 periods of quarter wavelength thick layers of AlAs(756 Å) and AlGaAs(650 Å) as the top mirror, $8^1/_2$ periods as the bottom mirror, and a spacer of $103^1/_2$ pairs of 100 Å GaAs quantum wells with 100 Å AlGaAs barriers. The top mirror was doped p-type with beryllium to approximately 1 x 10^{18} cm^{-3}, and the bottom mirror was doped n-type with silicon to approximately 1 x 10^{18} cm^{-3}. The spacer between the gratings was not intentionally doped. Device #2 has 9 and $12^1/_2$ periods for the top and the bottom mirror, respectively. The spacer layer has 38 quantum wells.

Fig.4 is a typical narrow band spectrum of Device #1, measured by a Perkin-Elmer λ-9 spectrophotometer with different voltages applied. The resonance shifts as the bias is applied, and this shift can be used to estimate the refractive index change by assuming a uniform index change between the old and new resonant wavelengths. However, the grating has a wavelength dependent reflection phase, which can be characterized by an effective grating length, L_{eff} [20], so the resonant mode shifts less than the refractive index shift:

$$\left(\frac{\Delta\lambda}{\lambda}\right)_{eff} = \left(\frac{\Delta n}{n}\right)\frac{L_c}{L_c + L_{eff}}, \qquad (14)$$

where L_{eff} is found to be approximately $3\lambda/n$. The other effect is the dispersion of the spacer medium. As the index increases, the mode would move to a longer wavelength. But the refractive index of GaAs decreases as the wavelength increases [18], if the photon energy is below the bandgap energy. So the net effect is less movement of the mode:

$$\left(\frac{\Delta\lambda}{\lambda}\right)_{disp} = \left(\frac{\Delta\lambda}{\lambda}\right)_{eff}\frac{1}{1 - \frac{\lambda}{n}\frac{dn}{d\lambda}}, \qquad (15)$$

where the shift of the resonant mode due to the dispersion, $(\Delta\lambda/\lambda)_{disp}$ is smaller than the expected shift from Eq.(7), because $dn/d\lambda$ is negative [18]. $(\Delta\lambda/\lambda)_{disp}$ is the measured quantity. The index shifts estimated from spectra like Fig.4 with Eqs.(7) and (8) were found to be well described by a quadratic electro-optic coefficient, S ($\Delta n = S n^3 E^2/2$ and E is the electric field) [12]. Another observation of Fig.4 is that the index shift has a maximum, which is 0.18% in the case of Device #1. The limitation of the index shift is because the index change

due to quantum well excitons is limited [21]. The experimental data are summarized in Table II in which we also list the device result of Ref.[8] as Device #3. E_{max} in Table II is the electric field just before the index shift becomes negative. Device #2 has a lower E_{max} because the operating wavelength is closer to the exciton line.

As the bias increases, the minimum reflectivity of the Fabry-Perot R_{min} at the new resonant position goes up due to the electroabsorption in the active region (as shown in Fig. 4). Eq.(1) can be used again to estimate the absorption, by assuming that R_{min}=0 at the original mode, and the phase is matched at the new mode:

$$\Delta\alpha = \frac{1}{L_c} \ln\left(\frac{1 - R\sqrt{\frac{R_{min}}{R}}}{1 - \sqrt{\frac{R_{min}}{R}}} \right), \qquad (16)$$

$$\approx \frac{1}{L_c} \sqrt{R_{min}} \frac{\pi}{F}, \qquad (16')$$

where $\sqrt{R_{min}/R}$ is assumed to be small in deriving Eq.(16'). Since $\sqrt{R_{min}/R}$ can be quite large, Eq.(16') tends to underestimate the loss modulation, as compared to Eq.(16). The estimated $\Delta\alpha$ is listed in Table II. The chirp parameter α_c can thus be obtained from Eqs.(14), (15) and (16). Near the maximum index shift, the chirp is approximately 1~2 as shown in Table II. Such an observation actually suggests that these devices could also be (more) effective in the transmission mode of operation.

Once the maximum index shift, Δn_{max} and the chirp, α_c are estimated, the validity of the *Modulation Design Equation*, Eq. (5) can be tested. In the last two rows of Table II, we have included the enhanced phase shift, $\Delta\Theta$ and the estimated R_{FP} after the field is applied. Good agreement is obtained. It should be noted that Eq. (5) can only be used to estimate the modulated reflection, R_{FP} but not the on/off ratio. The on/off ratio is more dependent on the design of balanced grating mirrors. As discussed in Section IV.3, the rise of the minimum reflectivity (which should be zero ideally) gets enhanced as the finesse increases, for a given design error.

V.2. High-Performance Fabry-Perot Modulator

In last year's report, we presented initial results on our novel Fabry-Perot reflection modulator. We had achieved a 2:1 on:off ratio at an applied voltage of 25 V. The FP cavity

Table II. Summary of parameters and performance of various devices. Methods of estimating the index and absorption changes are discussedin texts. The agreement between measured and estimated modulated reflection, RFP is good. The slightly higher estimated values may be due to the measured finesse is lower than expected, which could be caused by the somewhat unbalanced mirrors.

Device	#1	#2	#3
Device Design			
Periods of top grating	5	9	8
Periods of bottom grating	8.5	12.5	12.5
Cavity length(μm), L_c	2.07	0.78	1.32
Finesse, F	12	38	29
Measurements			
Wavelength (nm), λ	873	869	849
Minimum reflectivity, R_{min}	3.2%	~4%	10%
Modulated reflection, R_{FP}	26%	33%	55%
Finesse, F	9	30	22
Estimated Parameters			
Maximum index shift, Δn_{max}	0.18%	0.22%	0.22%
Absorption change (cm^{-1}), $\Delta\alpha$	660	462	1430
Chirp parameter, α_c	1.4	2.4	0.8
Maximum applied field (kV/cm), E_{max} , @ (V) volts	125(25)	90(7)	110(15)
Verification of Eq.(5)			
Effective phase shift, $\Delta\Theta$	0.65π	0.94π	1.25π
Estimated modulated reflection, R_{FP}	30%	37%	60%

used to make that device had a finesse of ~6. Over the course of the last year, we have reduced the drive voltage to 7 V for a 10:1 on:off ratio with a 3 dB insertion loss [22].

Here, we discuss devices with cavity finesses of 30-40. For one such cavity, the mirrors consist of multiple periods of AlAs-729 Å thick and $Al_{0.2}Ga_{0.8}As$-629 Å thick. The top mirror has 9 periods and the bottom mirror has 12.5 periods giving both mirrors a reflectivity of ~92%, balancing the resonator. It was designed to operate at 875 nm, sufficiently far from the exciton absorption edge at ~850 nm, yet close enough to it to make it possible to achieve a significant index modulation. The top mirror is doped p-type and the bottom mirror is doped n-type, making it possible to apply an electric field across the medium separating the mirrors of the FP. For the sample (FP1), the intracavity region ($3\lambda/n$ thick) consisted of 36 100 Å GaAs quantum wells separated by 100 Å $Al_{0.2}Ga_{0.8}As$ barriers with the outermost barriers adjusted to make the total thickness 0.76 μm. A scanning-electron microscope cross-section of FP1 is shown in Fig 8. Devices were fabricated by evaporating 100-200 μm wide ohmic contact

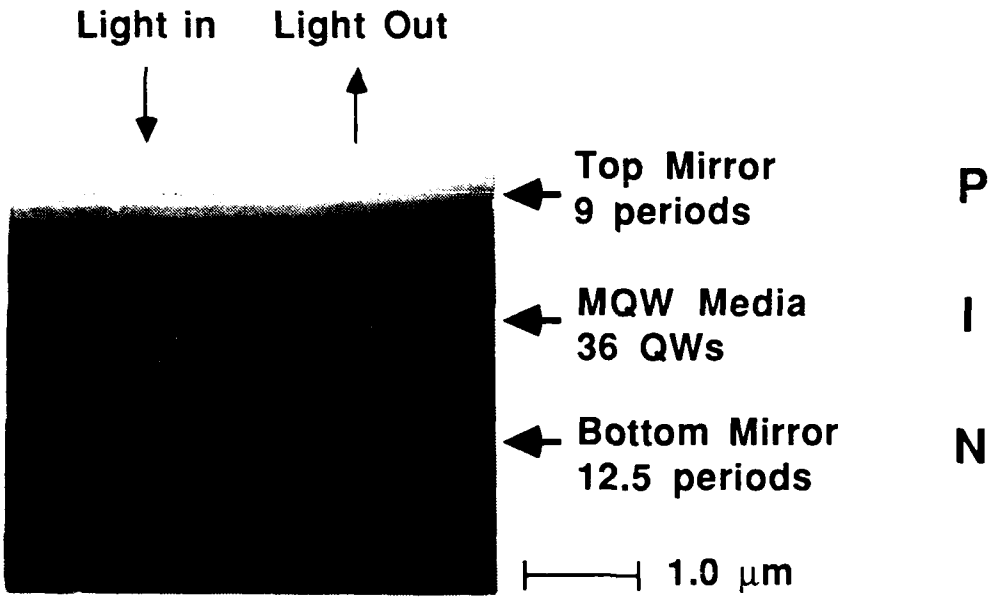

Figure 8: Scanning Electron Microscope Cross-Section of Fabry-Perot Modulator

stripes on the top surface and a broad-area contact on the back surface. Devices ~700 μm on a side were then cleaved for testing. In Fig. 9, we present a plot showing the theoretical reflectivity modulation, ΔR, vs. FP cavity length for different mirror combinations and drive voltages. Also plotted on Fig. 9 are experimental data which are in good agreement with the predicted values.

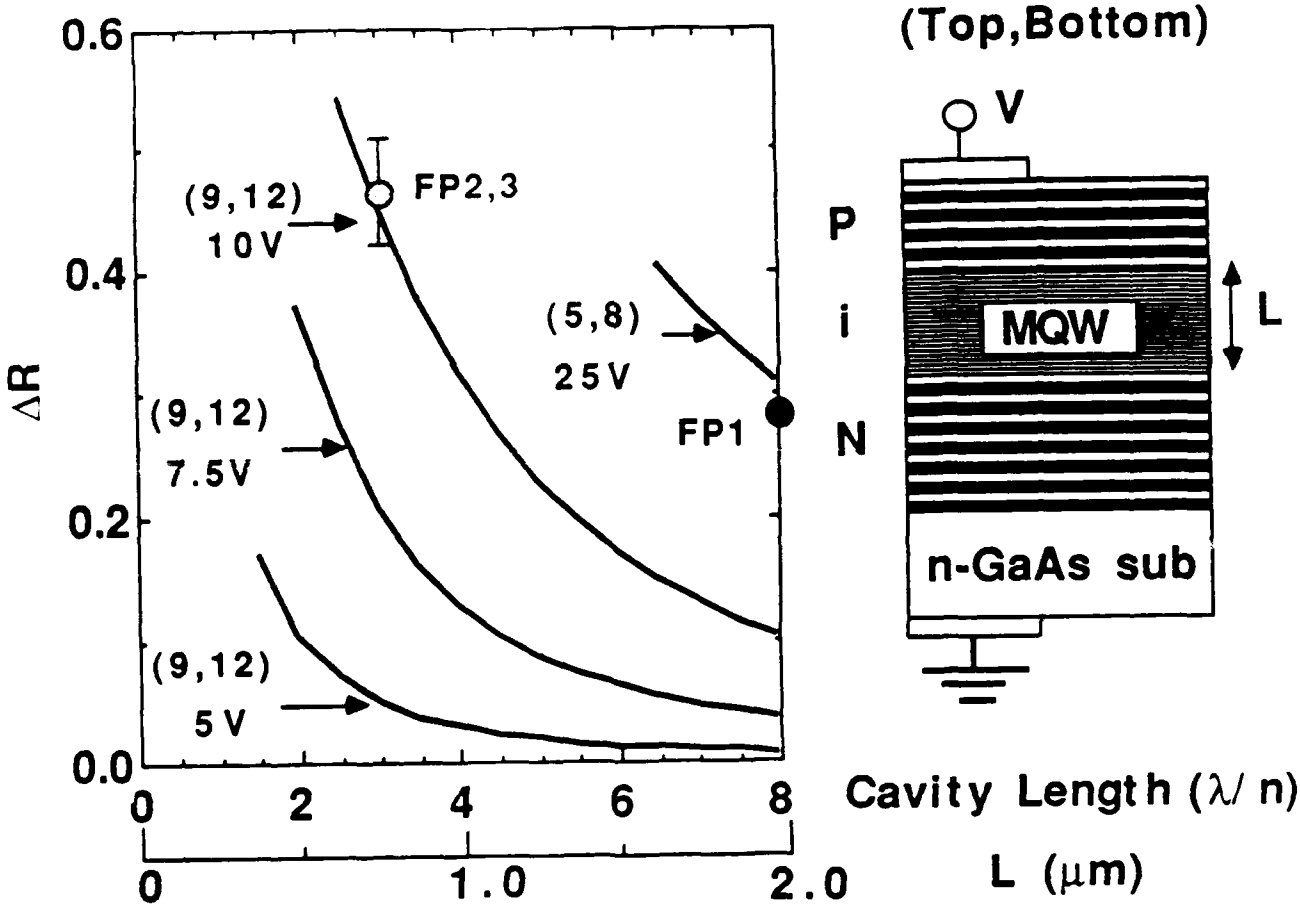

Figure 9 Reflectivity modulation vs. cavity length for various applied voltages and different mirror combinations. Numbers in parenthesis, (Top,Bottom) represent the number of quarter-wavelength periods used in the top and bottom grating, respectively. Data points summarize the experimental results, as well as the agreement between the theory and experiments. The maximum applicable field is limited to be 150 kV/cm which terminates the calculated curves.

In Fig. 10, we present a voltage-dependent reflection spectra for a device made from FP1. The zero-bias resonance full-width-at-half-maximum (FWHM) is 2.8 nm and minimum reflectivity is ~17%. Both values are larger than expected due to the aforementioned

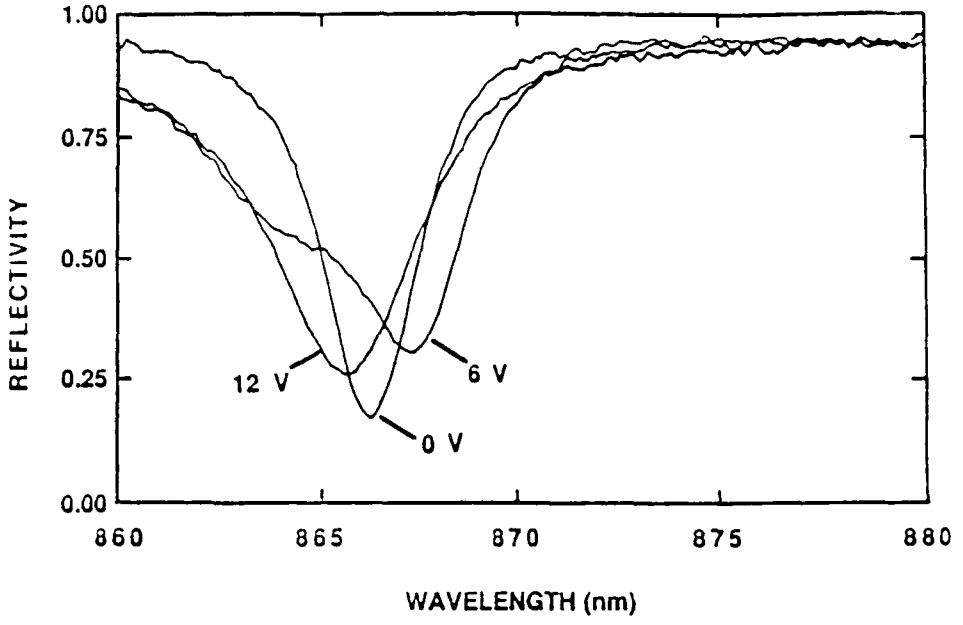

Fig. 10: Voltage dependent reflection spectra for Fabry-Perot device measured with insufficient resolution. We used a Perkin-Elmer Lambda-9 spectrophotometer to measure voltage dependent reflection spectra on the devices. For these measurements, the sample area was limited to an area 500 μm in diameter, and the angle of incidence was 10°. The non-Gaussian nature of the astimagtic beam in the spectrophotometer can induce a significant amount of spectral broadening of the FP resonances — we estimate it to be ~1.5 nm for the present structure — causing the measured resonances to be significantly broader than they the actually are and also causing the measured minima to be higher than they actually are.

broadening; an ideal structure would have a 2.0 nm FWHM and a 0% minimum reflectivity. The mode shifts first to higher wavelength and then to lower wavelength as the bias increases as expected [7]. The contrast ratio that can be inferred from the data is 2.5. We have measured the actual modulation performance with the dye laser system; the contrast ratio is actually 10 for a 7 V drive (the devices are always operated in reverse-bias mode). A scope trace for another device fabricated from the same area on the epi-layer operating at ~869 nm is shown in

Fig. 11a. It shows a contrast ratio of 12 for a 10 V drive. The total power switched is ~50 μW, and the insertion loss is < 3dB. We have observed some saturation in the modulation for higher power intensities. The modulation is due to both an index shift ($\Delta n/n \sim 0.24\%$) and an

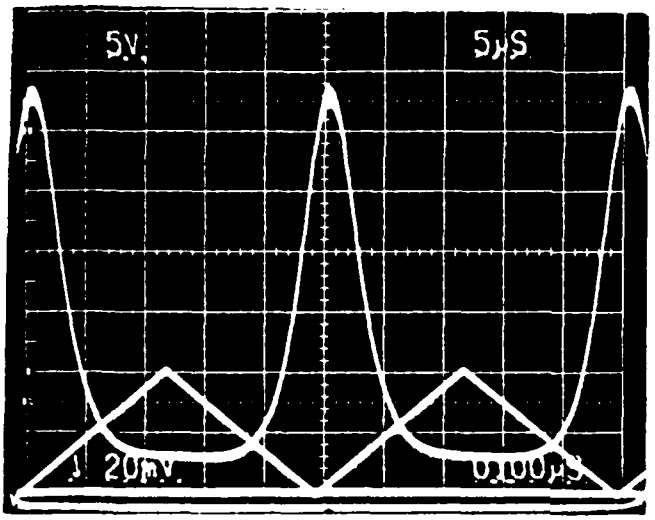

Fig. 11a: Reflection modulation with dye laser tuned at 869 nm, the minimum of reflection. The spot size used for the dye laser measurements is ~60 μm in diameter. The bottom line is optical ground and electrical -10 V. The top of the graph is ~50% reflection. The input signal is a 0 to -10 V triangular waveform. The optical intensity modulation is non-linear.

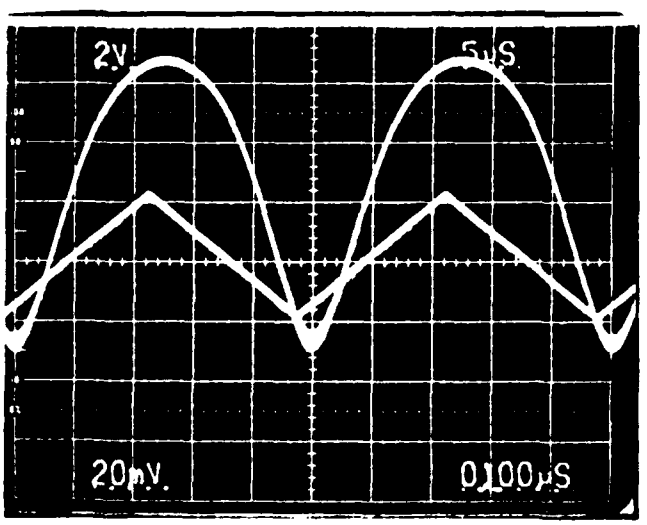

Fig. 11b: Reflection modulation also at 869 nm. The top line is optical ·d and electrical 0 V. The input ;ig...l is ٩ -6 to -10 V triangular waveforr Here, the modulation is more line .

absorption increase in the MQW media between the mirrors. Furthermore, spectrophotometer measurements show that the index shift is quadratic with electric field. In Fig. 11b, we present

the modulator performance with a 4 V peak-to-peak (ptp) ac signal imposed on a 8 V dc reverse bias . The contrast ratio is 9. Such a low drive voltage demonstrates that FP modulators do indeed offer promise as low-voltage optical modulators.

The low ac switching voltage demonstrates that the FP modulator can indeed perform as a low-power switch. We are currently fabricating small-area modulators to demonstrate that the high-speed performance predicted by theory can be achieved. For the material presented above with a 0.75 μm intrinsic region, the capacitance is ~1.5 x 10^{-4} pF/cm^2. Thus, a 25-μm diameter diode will have an RC-limited 3 dB roll-off frequency of ~ 40 GHz.

V.3. Comparison with other Modulators

On the next page in Table III, we present a comparison of our results achieved to date with the Fabry-Perot modulator [7,22] versus the results achieved by other groups with other modulator schemes[5,6,23,24]. Most of the other modulator presented in the table rely on a single- or double-pass absorption of light passing through a MQW layer. To achieve good performance, it is necessary to make the MQW region rather thick causing the drive voltages for these devices to be high. Because of the Fabry-Perot effect we are able to achieve high on:off ratios for modest drive voltages. There have also been several interesting theoretical studies made on all-semiconductor Fabry-Perot modulators [9,13].

V.4. Field-Induced-Stark-Localization of Superlattices

In the last year, we introduced a new concept which we refer to as Field-Induced-Stark-Localization of Superlattices or FISLS [25]. We apply an electric field across a superlattice consisting of GaAs/$Ga_{0.5}Al_{0.5}As$. The applied field breaks the energy degeneracy of tunneling coupled wells, removing the minibands formed by the original coupling. Since the miniband is centered at the nondegenerate energy level, a blue-shift in the absorption is expected. With the absorption change, we also observe an associated index shift. Data on the observed absorption and calculated index changes in a 36-period 30Å GaAs/25Å $Ga_{0.5}Al_{0.5}As$ superlattice are

Table III Comparison of UCSB Fabry-Perot Modulator Performance with results reported by other Laboratories.

Structure	MQW Fabry Perot	MQW Fabry Perot	Quarter-λ stack	MQW with integrated mirror	MQW	MQW	MQW
	UCSB	AT&T	Stanford	AT&T	Hughes	Rockwell -	Rockewell
Modulation Mechanism	index	index	index	two-pass absorption	absorption	two-pass absorption	absorption
Insertion Loss (dB)	3	3	5	6.2	13	4	2
Contrast Ratio	10:1	5:1	2.5:1	7:1	10:1	26:1	4.4:1
Drive Voltage (V)	7	17	100	18	20	24	20
Reference	[7]	[8]	[6]	[5]	[23]	[24]	[24]

presented in Fig. 12. We do observe a blue-shift of the absorption edge; the maximum absorption change, $\Delta\alpha$, is -3000 cm^{-1}, and the maximum index shift, Δn, is 0.01. A blue-shift may be very useful for the integration of in-plane integrated laser-modulators; with a FISLS-based modulator, it will be possible to eliminate absorption of the laser light in the modulator structure.

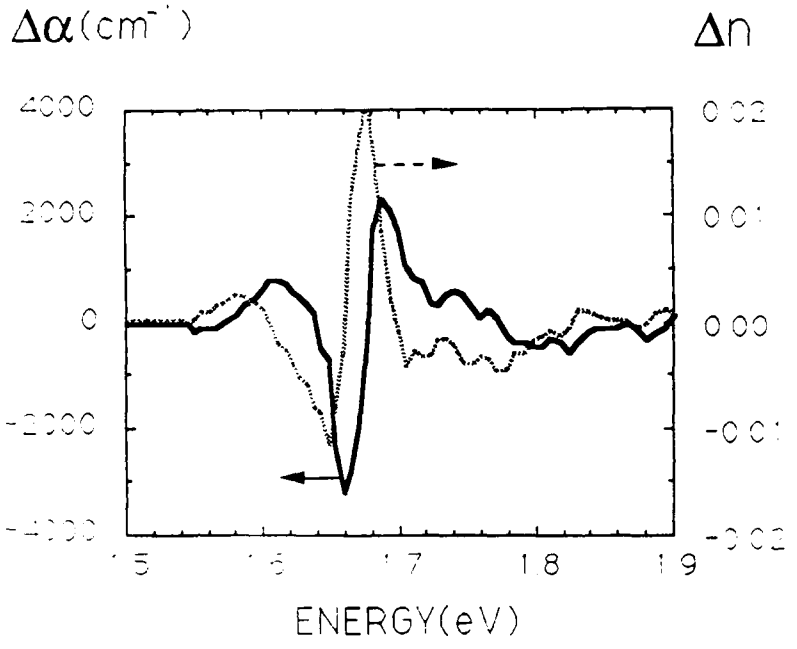

Fig. 12: Measured Change in loss, $\Delta\alpha$, and subsequently calculated change in refractive index, Δn VS energy for 36 period 30Å GaAs/25Å $Ga_{0.5}Al_{0.5}As$ superlattice structure discussed in the text.

V.5. Experimental Equipment

The following paragraph briefly mentions some of the new experimental systems that we have acquired or built in the last year. We received a commercial spectrophotometer (Perkin-Elmer Lambda-9); it is interfaced to an IBM computer. We use it to make wavelength-dependent reflection or transmission measurements for initial materials characterization. It has also proven useful for measuring device properties; however, because of its astigmatic beam, which can induce some broadening when measuring narrow resonances, it cannot be used to accurately measure the modulation properties of our new FP devices. Hence, we have recently

started using a tunable dye laser to measure the device modulation performance. In cooperation with Hewlett Packard, we are building a device measurement system built with a Leitz optical microscope. A laser source will be coupled into the microscope; using an IR vidicon camera, we will be able to quickly and easily align the measurement probe with very small devices. The reflected signal will be coupled back out of the microscope through the optical fiber used to couple it into the microscope. Finally, we have also put together a photo-current measurement system which allows us to make wavelength-dependent measurements to study the absorption properties our material.

The GaAs/AlGaAs epitaxial material for the work described was all grown in a Varian Gen II MBE system at UCSB. The system is now coming off bake-out after over one year of continuous operation under ultra-high vacuum conditions.

References

[1] P.L. Gourley and T. J Drummond, "Optical bleaching in an epitaxial (Al,Ga)As Fabry-Perot resonator," Appl. Phys. Lett. **51**, 1395 (1987).

[2] J.L. Jewell, A. Scherer, S.L. McCall, A.C. Gossard, and J.H. English, "GaAs-AlAs monolithic microresonator arrays," Appl. Phys. Lett. **51**, 94, (1987).

[3] J. Ohta, K. Kyuma, M. Oita, K. Mitsunaga, K. Hamanaka, and Y. Nakayama, "All-optical active switch using a multiple quantum well nonlinear etalon as a laser diode mirror," Electron. Lett. **24**, 216 (1988).

[4] T.H. Wood, C.A. Burrus, D.A.B. Miller, D.S. Chemla, T.C. Damen, A.C. Gossard, and W. Wiegmann, "131 ps optical modulation in semiconductor multiple quantum wells (MQW's)," IEEE J. Quantum Electron., **QE-21**, 117 (1985).

[5] G.D. Boyd, D.A.B. Miller, and D.S. Chemla, S.L. McCall, A.C. Gossard, and J.H. English, "Multiple quantum well reflection modulator," Appl. Phys. Lett. **50**, 1119 (1987).

[6] G.W. Yoffe, D.G. Schlom, and J.S. Harris, Jr., "Modulation of light by an electrically tunable multilayer interference filter," Appl. Phys. Lett. **51**,1876 (1987).

[7] R.J. Simes, R.H. Yan, R. S. Geels, L. A. Coldren, J. H. English, A. C. Gossard, and D. G. Lishan, "Electrically tunable Fabry-Perot mirror using multiple quantum well index modulation", Appl. Phys. Lett. **53**, 637 (1988).

[8] Y. H. Lee, J. L. Jewell, S. J. Walker, C. Tu, J. P. Harbison, and L. Tl Florez, "Electro-dispersive multiple-quantum-well modulator", Appl. Phys. Lett. **53**, 1684 (1988).

[9] D. R. P. Guy, N. Apsley, L. L Taylor and S. J. Bass, "Theory of an electro-optic modulator based on quantum wells in a semiconductor etalon", SPIE **792** Quantum Well and Superlattice Physics, 189 (1987).

[10] W. J. Gunning, "Electro-optic tuned spectral filters: a review", Optical Engineering, **20**,837 (1981).

[11] R. Lytel and G.F. Lipscomb,"Narrowband electrooptic tunable notch filter", Appl. Opt. **25**, 3889 (1986).

[12] R. H. Yan, R. J. Simes, R. S. Geels, L. A. Coldren, J. H. English, and A. C. Gossard, "Multi-quantum well electro-optic modulator using a combination of excitonic and absorption changes", 46th Annual Device Research Conference, Paper IVB-2, Boulder, Colorado, (1988).

[13] M. Whitehead, G. Parry, and P. Wheatley, IEEE Proceedings. **136** Pt. J, 52 (1989).

[14] J.P. van der Ziel and M. Ilegems, "Multilayer GaAs-$Al_{0.3}Ga_{0.7}As$ dielectric quarter wave stacks grown by molecular beam epitaxy," Appl. Opt. **14**, 2627 (1975).

[15] P.L. Gourley and T. J. Drummond, "Single crystal, epitaxial multilayers of AlAs, GaAs and $Al_xGa_{1-x}As$ for use as optical interferometric elements," Appl. Phys. Lett. **49**, 489 (1986).

[16] R. L. Thornton, R. D. Burnham, and W. Streifer, "High reflectivity GaAs-AlGaAs mirrors fabricated by metalorganic chemical vapor deposition", Appl. Phys. Lett. **45**, 1028 (1984).

[17] M. Born and E. Wolfe, "Principles of Optics", (Pergammon Press, Exeter, 1984).

[18] M. A. Aframowitz, "Refractive Index of $Ga_{1-x}Al_xAs$", Solid-State Communications, **15**, 59 (1974).

[19] H. A. Haus, "Waves and Fields in Optoelectronics", Ch. 3. (Prentice-Hall, Inc., New Jersey, 1984).

[20] Y. Suematsu, S. Arai, and K. Kishino, "Dynamic Single-Mode Semiconductor Lasers with a Distributed Reflector", J. Lightwave Tech. **LT-1**, 161 (1983).

[21] Y. Kan, H. Nagai, M. Yamanishi, and I. Suemune, "Field Effects on the Refractive and Absorption Coefficient in AlGaAs Quantum Well Structures and Their Feasibility for Electrooptic Device Applications", IEEE J. Quantum Electron. **QE-23**, 2167 (1987).

[22] R. J. Simes, R. H. Yan, D. G. Lishan, and L. A. Coldren, "High-Contrast Low-Voltage Fabry-Perot Reflection Modulator," submitted to the 15th European Conference on Optical Communication (1989).

[23]. T. Y. Hsu, U. Efron, W.-Y. Wky, J. N. Schulman, I. J. O'Haenens, and Y. C. Chang, Opt. Eng. **27**, 372 (1988).

[24]. R.B. Bailey, R. Sahai, and C. Lastufda, "1x16 Arrays of GaAs/AlGaAs Multiple Quantum Well Optical Modulators with 26:1 Contrast," Topical Meeting QW for Optics & Optoelectronics, Salt Lake City, paper PD1-1 (March 1989).

[25] R. H. Yan, R. J. Simes, H. Ribot, L. A. Coldren, and A. C. Gossard, "Blue-Shifted Absorption using Field-Induced Stark Localization in Superlattices," Topical Meeting QW for Optics & Optoelectronics, Salt Lake City, (March 1989).

VI. Conference and Journal Publications

[1] R. J. Simes, R. H. Yan, J. H. English, L. A. Coldren, and A. C. Gossard, "MBE-Grown Fabry Perot Multiple Quantum Well Reflection Modulator," J. Vac. Sci. and Tech., 7, (2) 412-414 (March/April 1989).

[2] R. J. Simes, R. H. Yan, R. S. Geels, L A. Coldren, J. H. English, A. C. Gossard, and D. G. Lishan,"Electrically Tunable Fabry-Perot Mirror using Multiple Quantum Well Index Modulation," Appl. Phys. Lett. **53,** 637 (1988).

[3] R.H. Yan, R. J. Simes, and L. A. Coldren, "Analysis and Design of Surface-Normal Fabry-Perot Electro-Optic Reflection Modulators," submitted for publication.

[4] R. J. Simes, R. H. Yan, R. S. Geels, L. A. Coldren, J. H. English, and A. C. Gossard, "Fabry-Perot multiple-quantum well index modulator," Appl. Optics **27,** 2103 (1988).

[5] R. H. Yan, R. J. Simes, R. S. Geels, L. A. Coldren, J. H. English, A. C. Gossard, and D. G. Lishan, "Electrically tunable Fabry-Perot mirror using multi-quantum well index modulation," Device Research Conference, Boulder, CO, paper IVB-2, (1988).

[6] R. J. Simes, R. H. Yan, R. S. Geels, L. A. Coldren, J. H. English, and A. C. Gossard, "Surface-Normal Fabry-Perot Multi-Quantum Well Index Modulator," CLEO 1988, Anaheim, CA (1988).

[7] R. J. Simes, R. H. Yan, D. G. Lishan, and L. A. Coldren, "High-Contrast Low-Voltage Fabry-Perot Reflection Modulator," submitted to the 15th European Conference on Optical Communication (1989).

[8]. R. H. Yan, R. J. Simes, H. Ribot, L. A. Coldren, and A. C. Gossard, "Blue-Shifted Absorption using Field-Induced Stark Localization in Superlattices," Topical Meeting QW for Optics & Optoelectronics, Salt Lake City, (March 1989).

[9]. R.H. Yan, R.J. Simes, H. Ribot, L.A. Coldren, and A.c. Gossard, "Room-temperature two-dimension exciton exchange and blue shift of absorption edge in GaAs/AlGaAs superlattices under an electric field." Appl. Phys. Lett., **54**, 1549 (1989).

VII. Personnel

1. Professor Larry A. Coldren, Ph.D.: Principal Investigator.
Dr. Coldren received his doctorate from Stanford University in 1972. He spent the next twelve years at Bell Labs before moving to the University of California at Santa Barbara in 1984. He holds 21 patents in the areas of surface-acoustic-wave signal processing devices, microfabrication processes and III-V compound optoelectronic devices for optical communication and processing. He has over 190 journal publications in these same areas. His current interests are in the areas of optical communication, optical computing and microfabricaion technology. In this project Dr. Coldren contributed the basic ideas and research management.

2. Mr. T.R. Hausken: Research Assistant.
Mr. Hausken received his B.S.E.E. from Montana State University in 1979. He spent the next five years at Texas Instruments first with ac plasma display development, and later with MOS memory failure analysis. He began studies at UCSB in 1/85 and was responsible for testing of optical devices.

3. Mr. R.J. Simes: Research Assistant.
Mr. Simes received his B.S. in Dec. 1983 from UCSB and started graduate studies immediately thereafter. His interests and contributions include molecular beam epitaxy of the surface-normal optoelectronic structures, and also their fabrication and testing.

4. Mr. R.H. Yan: Research Assistant.
Mr. Yan received his B.S. degree from National Taiwan University in 1984. He joined UCSB in 1986. His contributions included assisting in the development of the theory to model the D.E.T. phase modulator and design and testing of the surface normal modulator.